Positioning System for Particles in Microfluidic Structures

D. Kappe[1*], A. Hütten[1]
[1]Thin Films and the Physics of Nanostructures, Bielefeld University, Bielefeld, Germany
*Bielefeld University, 100131, 33501 Bielefeld, Germany, email: dkappe@physik.uni-bielefeld.de

Abstract: The possibility to detect and probe molecules in microfluidic devices gives rise to interesting applications. There are different approaches how to detect and probe particles, but a common step, for most methods, is to place the particles on a sensor. This can be done by applying external field gradients, or in this case by utilizing gravitational and hydrodynamic effects. Therefore, the sensor is placed beneath a microfluidic structure of changing height. Numerical simulations for various flow rates show, that the amount of captured material can be significantly increased in comparison to a straight channel. The geometry can be adapted to different flow rates, at the cost of higher aspect ratios and a longer ramp.

Keywords: Microparticles, Gravitation, Positioning

1. Introduction

Magnetic micro- and nanoparticles have gained a lot of interest during the last decades, due to a wide field of possible applications. They can be used as contrast agents for magnetic resonance imaging (Roch et al. [1]), as magnetic drug carrier (Lübbe et al. [2]) or for hyperthermia (Hergt et al. [3]) to destroy malignant cells by thermal heating. This is possible due to the fact, that magnetic particles can be manipulated by external fields. They are aligned to the direction of the field and for the case of an inhomogeneous field are exposed to an additional force. The stray field of such particles can also be detected by magneto-resistive sensors, using the stray field's effect on soft magnetic layers for example (Schotter et al. [4], Ferreira et al. [5], Besse et al. [6]). Both effects show high potential for lab-on-a-chip devices. Especially if biomolecules are combined with magnetic particles, they could be manipulated and detected (Panhorst et al. [7], Kinoshita et al. [8]). If additionally the surface of the sensor is functionalized in such a way, that specific biomolecules only bind at a specified locations, then the biomolecules could be distinguished between (Wang and Li [9]).

One problem of such devices is the rapid decay of the particles stray field. Therefore, the particle has to be placed close to the sensor at the bottom of the channel. There are different possible solutions to increase the probability of the particles reaching the sensor. One well known strategy is to pull the particles by applying a inhomogeneous magnetic field created by conducting lines (Brezska et al. [10]). But this solution has some disadvantages, like the complexity of the device being increased, and an additional magnetic field raising the noise signal of the sensor making the detection worse.
Another solution has been proposed by Weddemann et al. [11], which utilizes gravity and a change in the channels geometry. It was demonstrated in simulations and experiments that this approach works. In this work we rerun the simulations done previously and try to adapt this approach to problems with different parameters.

2. Governing equations

The velocity profile u of an incompressible fluid is described by the Navier-Stokes equation

$$\frac{\partial u}{\partial t} + (u\nabla)u = -\frac{\nabla p}{\rho} + \frac{\eta}{\rho}\,\Delta u + f, \qquad (1)$$

where p denotes the pressure profile, f the external force density and ρ and η the density and viscosity of the fluid. Furthermore the equation of continuity has to be considered, which simplifies to

$$\nabla \cdot u = 0 \qquad (2)$$

for incompressible liquids. Without varying external forces, the time derivative $\frac{\partial u}{\partial t}$ can be omitted and in case of laminar flow, the non-linear terms have a vanishing contribution. Finally equation (1) simplifies to

$$\nabla p = \eta\,\Delta u + \rho\, f. \qquad (3)$$

Particles suspended in such a liquid are exposed to a force **F** proportional to the velocity difference between the particle v and the surrounding fluid u. According to Stokes drag law, a spherical particle of radius r is exposed to a Force **F** of

$$\boldsymbol{F} = 6\pi\eta r(v - u). \qquad (4)$$

For particles on the micrometer scale and below, inertia effects can be omitted and the particles velocity is given by

$$v = u + \frac{\boldsymbol{F}_{\text{ex}}}{6\pi\eta r}, \qquad (5)$$

where $\boldsymbol{F}_{\text{ex}}$ combines all external forces. At this point only gravity and buoyancy are taken into account and finally the particles velocity v is

$$v = u + \frac{2r^2}{9\eta}\left(\rho - \rho_{\text{part}}\right) g\vec{e}_z, \qquad (6)$$

with g denoting the gravitational constant, ρ_{part} the particles density and $\vec{e}_z$ a normal unit vector along the z axis.

The particles behavior is described by an advection-diffusion equation to contribute to thermal motion of the particles

$$\frac{\partial c}{\partial t} + \nabla \cdot j = 0 \text{ with } j = D\nabla c - (u - g\vec{e}_z)c \qquad (7)$$

with $D = k_B T/(6\pi\eta r)$ the diffusion constant and k_B the Boltzmann constant and T Temperature of the system. As the velocity scale is much higher than the particles size, the diffusion term only contributes in regions close to the boundary.

3. Model

The geometry investigated is shown in Figure 1. The square-shaped channel, of $h_i = 50\mu m$ on the left, changes over a length of $l = 200\mu m$ to a channel of width $a_o = 300\mu m$ and height of $h_o = 15\mu m$. The aspect ratio, defined as $\chi = \frac{h_i a_i}{h_o a_o}$ is $\frac{5}{9}$ and equals the slowing down of the fluid, while passing the structure. Parts of the inlet and outlet channels are modeled too, so that the correct flow profile is received inside the ramp structure. This is due to simple boundary conditions on the inlet. Figure 2 (a) shows a flow profile that has not jet adapted to the boundary conditions and is distorted, whereas (b) is showing a typical flow profile.

The flow profile is calculated using the COMSOL Incompressible Navier-Stokes model with a linear solver. A No-Slip condition is applied to all boundaries, except the inlet, outlet and the plane of symmetry. The inlet has the Inlet – Velocity condition with a velocity v_{in}, the outlet has a Open boundary – Normal stress boundary condition with $f_0 = 0$ applied.

There are two different models in use to characterize the particles behavior. The first calculates the density of the particles on the ramp's floor and is described in the following section. The second mode, maps the height at the ramp's entrance to the ramp's floor which is described in section 3.2 and illustrated in Figure 3

The carrier liquid is assumed to be water at room temperature $T = 300K$ resulting in $\rho = 998.2\,\frac{\text{kg}}{\text{m}^3}$ and $\eta = 1.002$ mPa s. For the particle parameters, a density $\rho_{\text{part}} = 2.500\,\frac{\text{kg}}{\text{m}^3}$ and a diameter $d = 1\mu m$ are chosen.

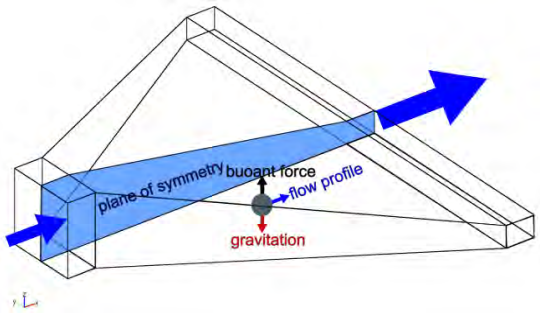

Figure 1. 3D Model of the ramp structure with all contributing effects. Gravitation (red), buoyancy (black) and flow profile (blue). Only half of the model is used for simulation purposes, as the model is symmetric.

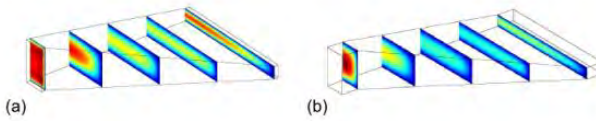

Figure 2. Simulation of the flow profile of a ramp structure. Entrance is $50\mu m \times 50\mu m$, outlet is $300\mu m \times 15\mu m$ with a ramp length of $200\mu m$. The length of the modeled inlet and outlet channels are (a) $5\mu m$ and (b) $20\mu m$

3.1 Concentration distribution

The concentration distribution is calculated with the COMSOL Convection and Diffusion Model, using artificial diffusion in a compensated Petrov-Galerkin framework. The physics are set according to equation (7). This model is only simulated for the ramp itself. The inlet boundary is set to a fix concentration of $c = c_0$, the outlet only allows convective transport, like the ramp's floor, which is equivalent to instantaneous bonding of particles. All other boundaries are set to an Insulation/Symmetry condition.

3.2 Initial height mapping

Like the concentration distribution this is calculated using COMSOL Convection and Diffusion Model. The mapping is illustrated in Figure 3. Every height at the entrance of the ramp is mapped to an area on the ramps floor where it is supposed to land. Therefore the boundary condition at the inlet is changed to $c = z$, shown at the inlet in Figure 3. This is equivalent to solving a level-set equation.

4 Results

As shown in Figure 4, the capturing rate of the structure compared to a straight channel is

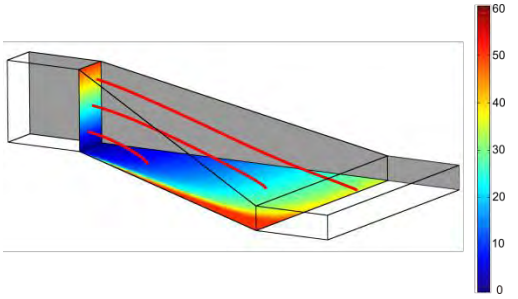

Figure 3. Simulation of the initial height mapping of a ramp structure. Entrance is $50\mu m \times 50\mu m$, outlet is $300\mu m \times 15\mu m$ with a ramp length of $200\mu m$. The length of the modeled inlet and outlet channels $20\mu m$. The streamlines show the path of a particle through the ramp while neglecting diffusion. The colors indicate, which height a particle needs at the entrance to land on the specified position. The gray boundary shows the plane of symmetry

increased significantly. The ramp collects more particles from higher initial heights, as shown in Figure 4b) and 4d). The channel achieves a maximum concentration of about 1.1 times the incoming concentration, in contrary the ramp has a maximum concentration of about 1.35 times the initial concentration which is an increase of about 22%. For lower velocities this effect is even bigger, which was investigated by Weddemann et al. [12]. Figure 4 shows solutions

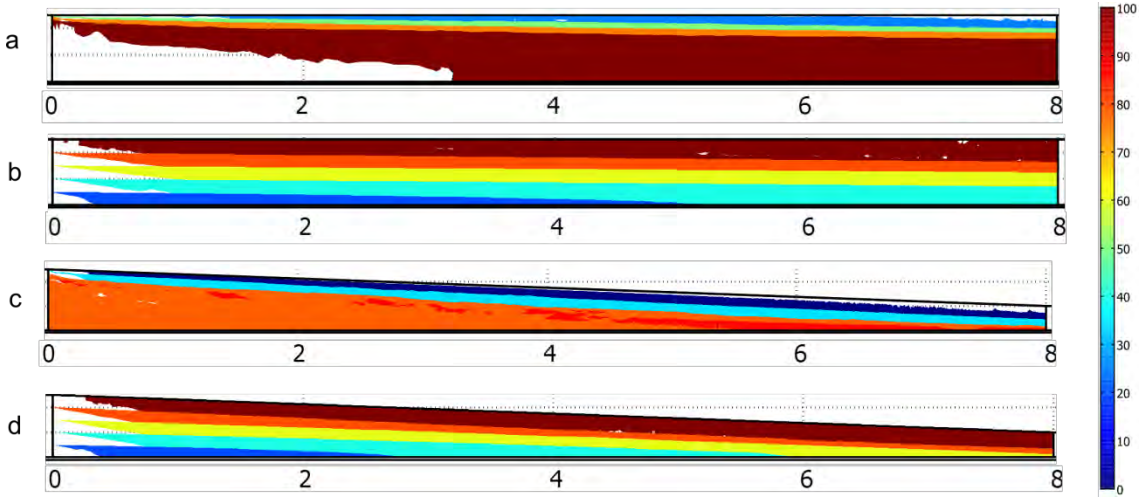

Figure 4. Comparison between a straight channel (a, b) and a ramp structure (c,d). Both models have a length of $800\mu m$ and an entrance of $80 \times 50\mu m$, the ramp structure ends with $400 \times 20\mu m$. Both are calculated for a fluid velocity of $250\ \mu m/s$. a) and c) show the concentration distribution of the respective structure, b) and d) are the corresponding height mappings.

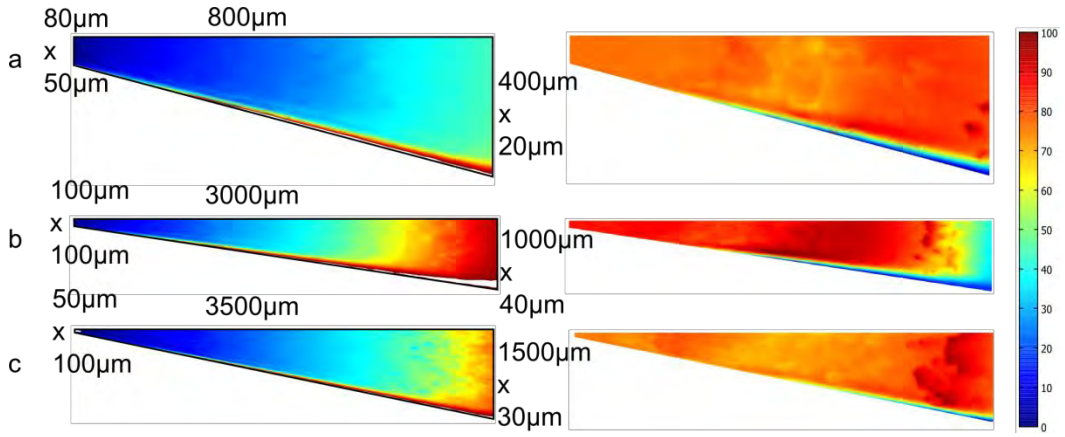

Figure 4. Simulations of the height mapping on the left side and the corresponding concentration distribution on the right side. The colors either indicate the initial height in percent of the total entrance height or the concentration in arbitrary units. The model geometries are given at the edges of the height mapping. From left to right it is entrance width × height, ramp length and exit width × height. The velocities are a) $250\mu m/s$ b) $500\mu m/s$ and c) $2500\mu m/s$

for different model geometries and higher velocities. Figure 4a) again shows the same ramp as Figure 3c) but a domain plot of the floor. The plot on the left shows the concentration distribution which has a minimum in the ramps center and a maximum afterwards. The choice of the model parameter mainly influences the position of the maximum of the concentration distribution. The model parameters can be adapted to a wide range of velocities, as Figure 4b) and 4c) show. For this cases the concentration on the floor are more homogenous as for a comparable channel structure and provide an 18% higher concentration peak. However this comes at a cost of high aspect ratios of the geometry making it more difficult to manufacture and to simulate. This can be observed in Figure 4c) where the resolution of the grid on the floor of the ramp is not sufficient. Additionally these ramps are much longer than those needed for slower fluid velocities.

5. Conclusion

The simulations show, that the model presented by A. Weddemann et al. [12] can be adapted to higher velocities. This comes at a cost of severe change in height and width of the structure. For simulations it is harder to find an appropriate mesh to get a good resolution of the floor on the one hand, and to reduce the calculation time needed on the other hand. The device can still be used to sort the incoming particles according to their height at the entrance of the ramps structure. COMSOL Multiphysics simulations provide estimates for efficient placement of the sensor inside the ramp structure.
For further studies of such models the mesh has to be improved to guarantee good resolutions of the floor even at high aspect ratios χ. Additional applications of the design, like a separation device, could be tested.

6. Acknowledgement

The authors would like to thank the BMBF project Bead Plus (16SV5403) for financial support.

6. References

[1] Roch A, Gossuin Y, Muller RN, Gillis P, Superparamagnetic colloid suspensions: water magnetic relaxation and clustering, *JMMM*, **293**, 532 (2005)
[2] Lübbe AS, Bergemann C, Huhnt W, Fricke T, Riess H, Brock JW, Huhn D, Preclinical experiences with magnetic drug targeting: tolerance and efficacy, *Cancer Res*, **56**, 4694 (1996)
[3] Hergt R, Dutz S, Muller R, Zeisberger M, Magnetic particle hyperthermia: nanoparticle

magnetism and materials development for cancer therapy, *J Phys Condens Matter*, 1**8**, 2919 (2006)
[4] Schotter J, Kamp PB, Becker A, Pühler A, Reiss G, Brückl H, Comparison of a prototype magnetoresistive biosensor to standard fluorescent DNA detection, *Biosens Bioelectron*, **19**, 1149 (2004)
[5] Ferreira HA, Graham DL, Parracho P, Soares V, Freitas PP, Flow velocity measurements in microchannels using magnetoresistive chips, *IEEE Trans Magn*, **40**, 2652 (2004)
[6] Besse PA, Boero G, Demierre M, Pott V, Popvic R, Detection of a single magnetic microbead using a miniaturized silicon Hall sensor, *Appl Phys Lett*, **80**, 4199 (2002)
[7] Panhorst M, Kamp PB, Reiss G, Brückl H, Sensitive bondforce measurements of ligand-receptor pairs with magnetic beads, *Biosens Bioelectr*, **20(8)**, 1685-1689 (2005)
[8] Kinoshita T, Seino S, Mizukoshi Y, Otome Y, Nakagawa T, Okitsu K, Yamamoto TA, Magnetic separation of amino acids by gold/iron-oxide composite nanoparticles synthesized by gammaray irradiation, *JMMM*, **293**, 106-110 (2005)
[9] Wang SX, Li G, Advances in giant magnetoresistance biosensors with magnetic nanoparticle tags: review and outlook, *IEEE Trans Magn*, **44**, 1687-1702 (2008)
[10] Brezska M, Panhorst M, Kamp PB, Shotter J, Reiss G, Pühler A, Becker A, Brückl H, Detection and manipulation of biomolecules by magnetic markers, *J Biotech*, **112**, 25-33 (2004)
[11] A. Weddemann, F. Wittbracht, A. Auge, A. Hütten, Positioning system for particles in microfluidic structures, *Microfluidics and Nanofluidics*, **7** ,849-855 (2009)